Journal of Biomolecular NMR **29:** 271–279, 2004.

NMR structural studies of domain 1 of receptor-associated protein

YiBing Wu[a,*], Molly Migliorini[b], Joseph Walsh[a], Ping Yu[a], Dudley K. Strickland[b,**] & Yun-Xing Wang[a,**]

[a]*Protein-Nucleic Acid Interaction Section, Structural Biophysics Laboratory, National Cancer Institute at Frederick, National Institutes of Health, Frederick, MD 21702, U.S.A.;* [b]*Department of Vascular Biology, Jerome H. Holland Laboratory for Biomedical Science, American Red Cross, Rockville, MD 20855, U.S.A.*

Received 10 November 2003; Accepted 29 December 2003

Key words: α-helix, dipolar couplings, RAP, receptor-associated protein

Abstract

The 39 kDa receptor-associated protein (RAP) is an endoplasmic reticulum resident protein that binds tightly to the low-density lipoprotein receptor-related protein (LRP) as well as to other members of the low-density lipoprotein receptor superfamily. The association of RAP with LRP prevents this receptor from interacting with ligands. RAP is a three-domain protein that contains two independent LRP binding sites; one located within domains 1 and 2, and one located within domain 3. As the first step toward defining the structure of the full-length protein and understanding the interaction between RAP and this family of receptors, we have determined the 3D structure of domain 1 using constraints derived from heteronuclear multi-dimensional NMR spectra, including NOEs, dihedral angles, J-couplings and chemical shifts, as well as two sets of non-correlated residual dipolar couplings measured from the protein solutions in anisotropic media of Pf1 and 6% polyacrylamide gel. The backbone C_α rmsd between the current structure and a homo-nuclear NOE-based structure is about 2 Å. The large rmsd mainly reflects the significant differences in helical orientation and in the structural details of the long helix (helix 2) between the two structures.

Introduction

The 39 kDa receptor-associated protein, RAP, is an endoplasmic resident protein that binds with a high affinity ($Kd \sim 0.6$–1 nM) to several members of the low-density lipoprotein (LDL) receptor family. This receptor family contains at least 13 family members, including the LDL receptor-related protein (LRP) /α2-macroglobulin receptor (α2MR), LRP1B, gp330/megalin, LDLR, the very low-density lipoprotein receptor (VLDLR) and apoE receptor 2. RAP functions as a molecular chaperone for LRP and other LDL receptor family members by binding to the newly synthesized receptors and preventing them from associating with ligands also present within the ER and by facilitating delivery of the receptors to the cell surface (Herz et al., 1991; Williams et al., 1992; Biemesderfer et al., 1993; Bu et al., 1995; Willnow et al., 1996).

Members of the LDL receptor family play important roles in cargo transport and in cell signaling events. LRP recognizes over 30 ligands, and functions in protease and lipoprotein catabolism. LRP also alters the trafficking and degradation of β-amyloid precursor protein (Kounnas et al., 1995), both of which are central to the pathogenesis of Alzheimer's disease. Mice deficient in RAP have decreased expression of LRP in the brain and liver (Willnow, 1995) revealing a critical role for RAP in the folding and delivery of LRP to the cell surface. Impaired function of RAP therefore could contribute to disease, and indeed, when RAP-deficient mice were crossed with human β-amyloid precursor protein transgenic mice, increased extracel-

*Present address: Department of Biochemistry & Biophysics, School of Medicine, 405 Mary Ellen Jones Building CB #7260, University of North Carolina at Chapel Hill Chapel Hill, NC 27599-7260, U.S.A.

**To whom correspondence should be addressed: E-mails: strickla@usa.redcross.org; wangyu@ncifcrf.gov

lular amyloid deposition was noted (Van Uden et al., 2002).

Despite wide interests in RAP, there has been no experimentally determined 3D structural information available for intact RAP, primarily due to the difficulty of obtaining a crystal for X-ray crystallography. The full-length RAP protein exhibits a non-NMR friendly solution behavior such as extensive chemical shift overlap and signal line broadening in an NMR test tube. As part of a larger effort, we have adopted a divide-and-conquer strategy to solve the structures of individual domains of RAP, since RAP is a modular protein (Medved et al., 1999). The 3D structure of the full-length RAP molecule may then be obtained using experimental restraints such as NOEs for the translational constraints, dihedral angle and chemical shift constraints, and residual dipolar couplings (RDCs) for orientational constraints.

Although a homonuclear NOE-based NMR structure of a similar D1 construct has been reported previously (Nielsen et al., 1997), the quality factor (Bax et al., 2001) is over 0.4 calculated using two sets of uncorrelated dipolar couplings that were measured in two different alignment media. A more accurate structure of D1 is required when orienting the domain in the structure determination of the full-length RAP or comparing the free D1 structure with that in the bound state with receptor fragments or docking to an antibody combining site (Janin and Chothia, 1990). Here we report the structure of D1 that was determined using traditional NMR constraints as well as RDCs. This D1 structure constitutes an initial step towards structure determination of the full-length RAP and understanding of the interaction between the RAP and certain LDL receptor family members.

Materials and methods

Sample preparation and chemical shift assignments of D1 have been reported previously (Medved et al., 1999, Wu, 2003). RAP is a modular protein containing three domains. In preparation of the protein samples, we made effort to investigate if there is any interaction between D1 and D2 to alter the structure of D1 when it is alone in solution. Our results show that there is no detectable interaction between D1 and D2 (Figure 1, supplementary materials). All experiments were recorded at 25 °C on Varian *INOVA*, 600 and 800 MHz spectrometer equipped with Z-gradient HCN-triple probes and a Varian *INOVA* 500 MHz

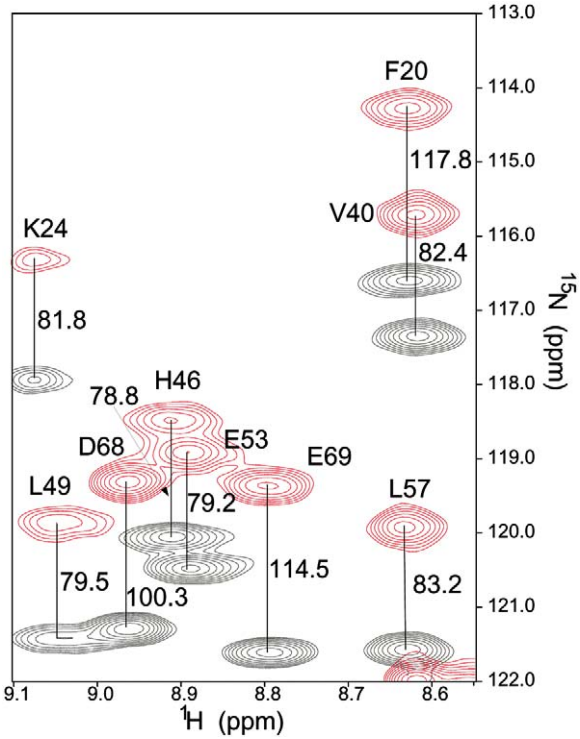

Figure 1. A superposed in-phase and anti-phase HSQC-IPAP spectra of D1 in 9.5 mg/ml Pf1 medium recorded on the spectrometer operating at proton frequency of 500 MHz. The data matrix is 1024 (t1)× 128 (t2) with 8 scan per FID.

spectrometers with a cryogenic Z-gradient HCN-triple probe. We used NMRPipe (Delaglio et al., 1995) and Pipp (Garrett et al., 1991), both running on SGI octane workstations, for NMR data processing and analysis.

We recorded a 3D ^{13}C-edited, a 3D ^{15}N-edited NOESY and a 3D ^{13}C/^{15}N-edited NOESY spectrum with a mixing time of 120 ms to obtain distance constraints, and an HNHA spectrum to extract JHNHA couplings. Distance calibration of the interproton distance constraints was done following the reported protocol (Garrett et al., 1997). The NOE constraints were grouped into four ranges, 1.8–2.7 Å (1.8–2.9 Å for NOEs involving NH protons), 1.8–3.3 Å (1.8–3.5 Å for NOEs involving NH protons), 1.8–5.0 Å, and 1.8–6.0 Å, corresponding to strong, medium, weak, and very weak NOEs respectively. Distances involving methyl groups, aromatic ring protons, and non-stereospecifically assigned methylene protons were represented as a $(\Sigma r^{-6})^{-1/6}$ sum (Nilges et al., 1988). Approximate χ_1 torsion angle ranges were obtained using HNHB and HACAHB spectra, combined with semi-quantitative analysis of the NOE spectra (Archer et al., 1991). Besides NOEs in-

volving side-chain protons and χ_1 torsion angles, we made no other attempt to extract constraints to restrict side-chains. The ϕ and ψ dihedral angle constraints were derived using a combination of CSI, quantitative analysis of JHNHA couplings (Vuister and Bax, 1994) and output values from the TALOS program (Cornilescu et al., 1999). Hydrogen bond constraints, two for each hydrogen bond (NH-O = 1.5–2.8 Å and N-O = 2.4–3.5 Å), were derived from NH exchange experiments, backbone NOE patterns and backbone C_α/C_β chemical shifts and applied in the later stage of the structure calculation. The backbone $C\alpha/C_\beta$ chemical shifts were also used directly in the structure calculation. Tight turns clearly identified by NOE patterns and J-coupling constants were restrained to their standard values with a $\pm 30°$ error range.

The RDCs were extracted from the difference in J-splittings measured in isotropic and anisotropic samples. We used two different alignment media: 9.5 mg Pf1/ml, and radially compressed 6% polyacrylamide (PA) gel (Chou et al., 2001). The protein does not interact with either alignment media significantly as judged by the comparison of ^{15}N-HSQC spectra taken in an/isotropic media. In preparation of Pf1-anisotropic D1 solution, a Pf1 stock solution of 50 mg/ml was filtered extensively with the buffer (50 mM NaCl, 75 mM NaPi, pH 7.25) using a 100 kDa molecular cut-off spin-filter. The volume of the protein-Pf1 solution was adjusted to attain an apparent concentration of $\sim$9.5 mg Pf1/ml based on a dilution factor and the sample induced a deuterium splitting of $\sim$ 14 Hz. (This large splitting suggests that the actual concentration of Pf1 in solution might be higher than that estimated based on dilution.) For the compressed PA gel, we cast 350 µl 6% arcrylamide solution (acrylamide:bis 25:1) in a casting cylinder with 0.599 cm inner-diameter and allowed it to polymerize overnight. The remaining procedures including drying, soaking the protein solution and transferring to a 5 mm NMR tube were the same as described in literature (Chou et al., 2001). In addition, we have also tested DMPC/DHPC liquid crystal media but observed no significant alignment of D1 at lipid concentrations below 15%.

$^1D_{\mathrm{NH}}$, $^1D_{\mathrm{C\alpha C'}}$ and $^1D_{\mathrm{C\alpha H\alpha}}$ were extracted from 2D ^{15}N HSQC-IPAP, 3D HNCO-JCOCA and 3D HN(CO)C–JCAHA respectively (Bax et al., 2001). Except for 2D ^{15}N HSQC-IPAP, which was recorded on spectrometers operating at proton frequencies of both 500 and 800 MHz, all others were performed on the 500 MHz spectrometer. Measuring $^1D_{\mathrm{C\alpha C'}}$ on a 500 MHz spectrometer offers advantages over the higher field spectrometer because CSA is a dominant relaxation mechanism in the ^{13}C′ T_2. A small region of the 2D ^{15}N HSQC-IPAP and a section of the strips from the 3D HN(CO)C–JCAHA spectra are shown in Figures 1 and 2. In processing the data, indirect-detected dimensions were linearly predicted to double the matrix size.

We used a combination of simulated annealing refinement together with a grid search (Clore et al., 1998b) and the histogram (powder-pattern) of $^1D_{\mathrm{NH}}$ and normalized $^1D_{\mathrm{C\alpha C'}}$ and $^1D_{\mathrm{C\alpha H\alpha}}$ (Clore et al., 1998a) to extract axial and rhombic components D_a and R, respectively. The approximate values of D_a and R of D1 in Pf1 and 6% PA were determined from the normalized distribution of all observed RDCs (Figure 3). The initial D_a and R were estimated to be about 17 Hz and 0.2, respectively in Pf1, and 20 Hz and 0.5, respectively in the radially compressed 6% PA. The final values of D_a and R were obtained from the simulated annealing refinement along with a grid search to yield values that give the lowest energy structures. D_a and R values are 19 Hz and 0.15 in Pf1 and 20 Hz and 0.65 in 6% PA, respectively. We would like to point out that the initial estimate of D_a and R for the alignment tensor in Pf1 was uncertain because there is only one large dipolar coupling at one of extremes, ca. -35 (-30) Hz of the normalized measured (calculate) $^1D_{\mathrm{C\alpha H\alpha}}$ of Phe20, and is away from the rest of the histogram. The measured T_1/T_2 and hetero-^{1}H-^{15}N NOE indicate that this residue has similar dynamics as those in the helices, and the sequential NOE-pattern of this region seems to indicate that Phe20 is not in random coil but in the middle of a small segment of α helix-like structure (residues 19–22). We estimated the R-value with and without the input from Phe20 and the resulted R-value ranges from 0.2 to 0.4. Using the simulated annealing refinement and grid search yields the best R-value of 0.15.

We calculated the structure of D1 using simulated annealing in torsion angle space (Stein et al., 1997) starting from an extended strand, followed by simulated annealing in Cartesian space using XPLOR-NIH 1.0.6, containing pseudopotentials for residual dipolar couplings, a conformational database and chemical shift refinement module (Schwieters, 2003). Molecular models were generated with Quanta (MSI).

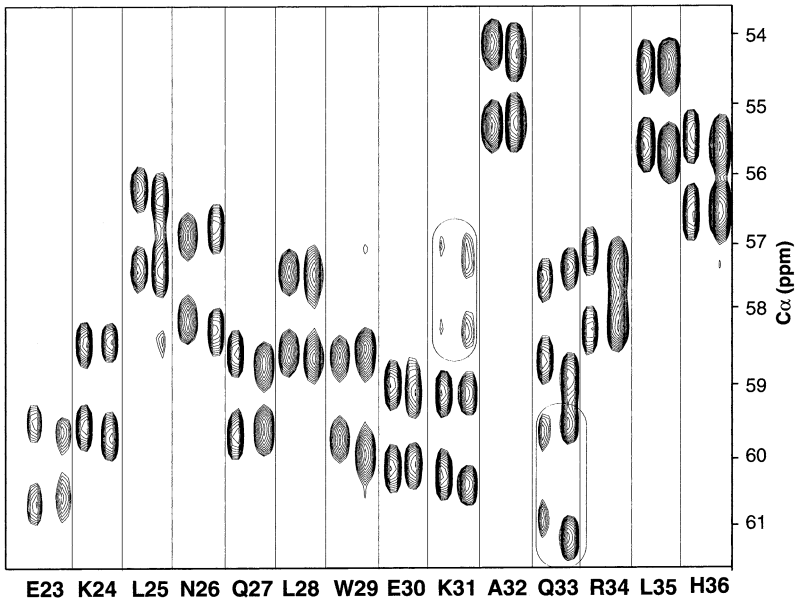

Figure 2. Small section taken from the 3D HN(CO)C–JCAHA spectra for the residues from E23 to H36 in helix 1, showing $^{13}C_{\alpha}$-($^{1}H_{\alpha}$) doublets in isotropic (left) and in 6% PA (right) on the right. The circled cross peaks are from adjacent 3D plans.

Results and discussion

Structure validation

RAP is a modular protein containing three domains. In preparation of the protein samples, we made effort to investigate if there is any interaction between D1 and D2 to alter the structure of D1 when it is alone in solution. Our results show that there is no detectable interaction between D1 and D2 (Figure 1, supplementary materials). The quality of the D1 NMR structure can be assessed using both Pearson's correlation coefficient, R_p, and a quality factor, Q-factor (Bax et al., 2001). R_p expresses the degree of linear relationship between two sets of variables, in this case, measured and calculated RDCs based on the structure. For a perfect linearity, R_p is equal to 1.0. Since the two sets of RDCs measured in the two media are not clearly correlated (Figure 4), the calculated structure using only Pf1 dipolar couplings is found to be in good agreement with the experimental RDCs measured in the 6% PA with $R_p = 0.94$. Figure 5 shows a correlation between the $^{1}D_{C\alpha H\alpha}$ couplings measured in the 6% PA vs. those best fitted to the structure refined with Pf1 RDCs (in addition to the NOE and dihedral angle constraints). The same analysis was performed with $^{1}D_{C\alpha H\alpha}$ couplings measured in the Pf1 vs. those refined using the structure generated based on the 6% PA RDCs and gave essentially the same R_p value. These two analyses suggest not only that the two sets of RDCs validate the structure but also the RDCs measured in Pf1 and the 6% PA are consistent with each other, indicating neither alignment media alters the D1 structure significantly.

$$Q = \mathrm{rms}(D_{\mathrm{meas}} - D_{\mathrm{pred}})/\mathrm{rms}(D_{\mathrm{meas}}).$$

The Q-factor, analogously to the crystallographic free R-factor, is another indicator of the quality of an NMR structure. We calculated the Q-factor in two ways. First, we used the lowest-energy structure calculated with the full set of RDCs from one medium along with traditional constraints to predict those in the second medium and to derive the Q-factor. The calculation was repeated for the structure generated using the RDCs from the second medium. The average Q-factor from the two calculations is 0.35. Second, we used the same method described by Ramirez et al. (2000) for cross validation. In this method, five subsets of $\sim 10\%$ of total RDCs of mixed types from both media were randomly selected. When a selected coupling is available for both Pf1 and 6% PA media, the subset includes both. The five structures calculated separately using all experimental constraints, but excluding one subset at a time, were used to predict those unused RDCs, and yielded an average Q-factor of 0.31. The better Q-factor calculated using this method is expected since only 10% of the total RDCs were excluded in each calculation whereas in the first method, all RDCs

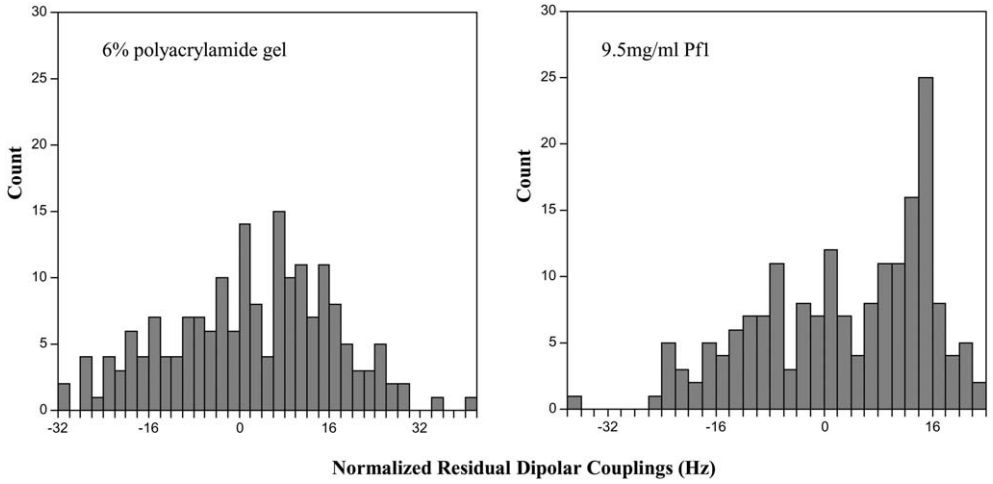

Figure 3. Histogram of the normalized ${}^1D_{\mathrm{NH}}$, ${}^1D_{\mathrm{C\alpha C'}}$ and ${}^1D_{\mathrm{C\alpha H\alpha}}$, measured in 6% PA (left) and 9.5 mg/ml Pf1 (right) alignment media, with scaling factors of 1, 5.05 and 0.498 respectively (Bax et al., 2001). Note on the left that the lone extreme value RDC measured in Pf1 is the normalized ${}^1D_{\mathrm{C\alpha H\alpha}}$ of Phe20 (see the discussion in the text).

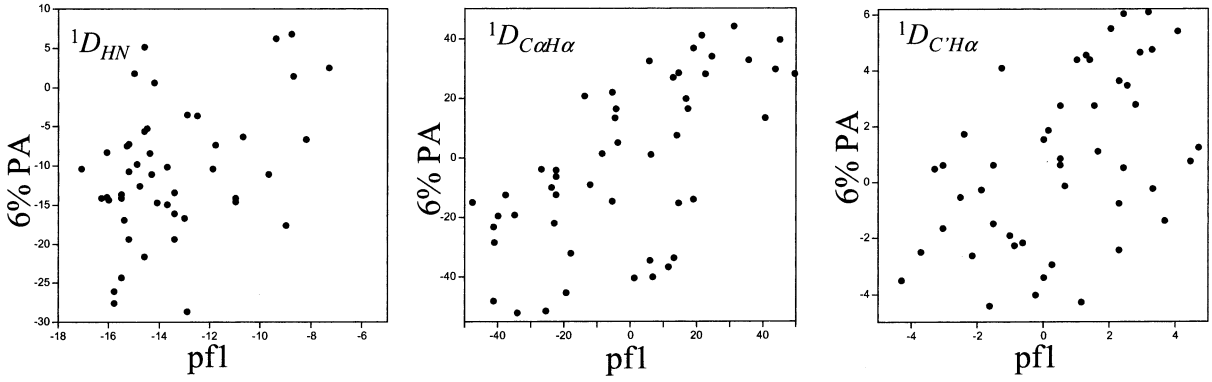

Figure 4. Plot of RDCs measured in 6% polyacrylamide gel vs those measured in ∼9.5% mg/ml Pf1. The Pearson correlation coefficient beween the two data sets is ∼0.66 and the normalized scalar product is ∼0.88 (see the text for the discussion). The lack of correlation between the two sets of data indicates two independent alignment tensors. In the Pf1 alignment tensor frame, the 6% PA alignment tensor is characterized by Euler angles $\alpha = 9°$; $\beta = 10°$; $\gamma = 71°$.

measured in one of two media were excluded from the calculation.

The R-value of D1 in Pf1 is ∼0.15. R is interpreted as an alignment asymmetry parameter. When the R-value approaches zero, the Euler angle γ is not well-defined (Mueller et al., 2000). Any rotation of a bond vector around the Z-axis of the alignment frame will yield an orientation that is consistent with the dipolar coupling data. One way to resolve this problem is to use a tailored algorithm (Mueller et al., 2000) that heavily depends on the accuracy of NOE-based initial structure and is sensitive to the errors in the values of axial and rhombic components. In the case of D1, we chose to obtain the second alignment frame from the dipolar couplings measured in 6% extruded PA gel to reduce ambiguity. The two sets of dipolar couplings measured from the media are independent from each other as evidenced by the lack of correlation shown in Figure 4. Using a grid search that minimizes the difference between the measured and predicted dipolar couplings (Tjandra and Bax, 1997), we obtained the alignment tensors that are characterized by Euler angles $\alpha = 112°$; $\beta = 93°$; $\gamma = 53°$ for Pf1 and $\alpha = 121°$; $\beta = 103°$; $\gamma = 124°$ for 6% PA.

It is worth to mention that cross-validation using two sets of RDCs is valid only when the two sets of data measured in two different alignment media are not correlated. The correlation can be assessed using Pearson's correlation coefficient between the two sets of RDCs or the normalized scalar product between

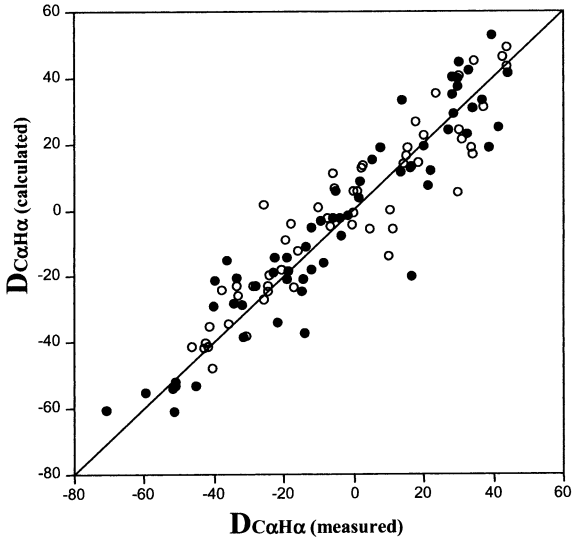

Figure 5. Correlation between $D_{C\alpha H\alpha}$ values measured in one alignment medium and predicted based on the structure refined with the RDCs from the second medium. The filled dots (open dots): $D_{C\alpha H\alpha}$ measured in Pf1 (PA) vs. $D_{C\alpha H\alpha}$ predicted by the structures refined with RDCs from PA (Pf1). The Pearson's correlation coefficient Rp for both is ∼0.93.

vectors of their irreducible representations of Saupe matrix (Sass et al., 1999). In the D1 case, the Pearson's correlation coefficient of the two sets of RDCs is ca. 0.66 and the normalized scalar product is ca. 0.88 (Saupe matrix note, supplementary materials). A value of 0 and 1.0 of the normalized scalar product means orthogonal and co-linear of two alignment tensors (Sass et al., 1999). The apparent high value of the scalar product in D1 is in part due to the near co-linearity between the z-axes between the two alignments.

Structure of D1

Excluding the 10 C-terminal residues, on average each residue contains ∼20 restraints. A superposition of the 20 final simulated annealing structures is shown in Figure 6. Backbone and non-hydrogen atom rmsds relative to the average structure are 0.21 ± 0.04 and 0.81±0.06 Å, respectively, and they have a good covalent geometry and reasonable energy terms (Table 1). Although the rmsd of the backbone in the ordered region is very low (high precision), rmsd of all heavy atoms is considerably higher. This is expected since no effort was made to obtain extensive constraints to restrain the side chains. The structural part of D1 consists of three roughly anti/parallel α-helices connected by two turns (Figure 7). Using PROCHECK, we derived the secondary structure boundary for the

Table 1. Restraints and structural statistics of domain 1 of RAP

A. Total restraints	1692	
Total distance restraints	1057	
Intraresidue (i=j)	134	
Sequential ($\|i-j\|=1$)	285	
Short range ($1<\|i-j\|\leq 4$)	367	
Long range ($\|i-j\|>4$)	219	
H-bond	52	
Total dihedral restraints	157	
ϕ	55	
ψ	55	
χ_1	47	
Total dipolar coupling constraints	320	
$^1D_{NH}$ (pf1)	53	
$^1D_{NH}$ (PA)	50	
$^1D_{C\alpha H\alpha}$ (pf1)	53	
$^1D_{C\alpha H\alpha}$ (PA)	55	
$^1D_{C'C\alpha}$ (pf1)	57	
$^1D_{C'C\alpha}$ (PA)	52	
Secondary chemical shifts	158	
$\delta_{C\alpha}$	79	
$\delta_{C\beta}$	79	
NOE violations >0.5 Å	0	
Dihedral angle violations >5°	0	
B. RMSDs		
Deviation from idealized geometry	{SA}	
Bonds (Å)	0.0039	± 0.0001
Angles (deg.)	1.42	± 0.02
Impropers (deg.)	0.93	± 0.02
Backbone (22-88) RMSD (Å)	0.24	± 0.05
Nonhydrogen. atoms (22-88) (Å)	0.80	± 0.06
RMSD from residual dipolar coupling (Hz)		
$^1D_{NH}$ (pf1)	1.23	± 0.05
$^1D_{NH}$ (PA)	1.12	± 0.09
$^1D_{C\alpha H\alpha}$ (pf1)	2.10	± 0.06
$^1D_{C\alpha H\alpha}$ (PA)	2.92	± 0.07
$^1D_{C'C\alpha}$ (pf1)	1.09	± 0.02
$^1D_{C'C\alpha}$ (PA)	1.34	± 0.03
C. Energies		
E(NOE) (kcal/mol)	121.13	± 10.7
E(dihed.) (kcal/mol)	7.92	± 0.82
E(repel) (kcal/mol)	199.0	± 28.35

{SA} is the ensemble of 20 lowest energy structures. With the exception of the residual dipolar coupling restraints, the values for the force constants applies for the various terms in the potential function used for the simulated annealing are the same as Bewley et al. (1998). We used an NH residual dipolar force constant of 1 kcal/mol.Hz^2 for pf1 derived $^1D_{HN}$ dipolar coupling restraints, 0.495 kcal/mol.Hz^2 for $^1D_{C\alpha H\alpha}$ dipolar coupling restraints and 1.98 kcal/mol.Hz^2 for $^1D_{C'C\alpha}$ dipolar coupling restraints. The force constants were timed by 0.7 and used for the dipolar restraints measured in 6% PA, to roughly account for the stronger alignment I 6% PA.

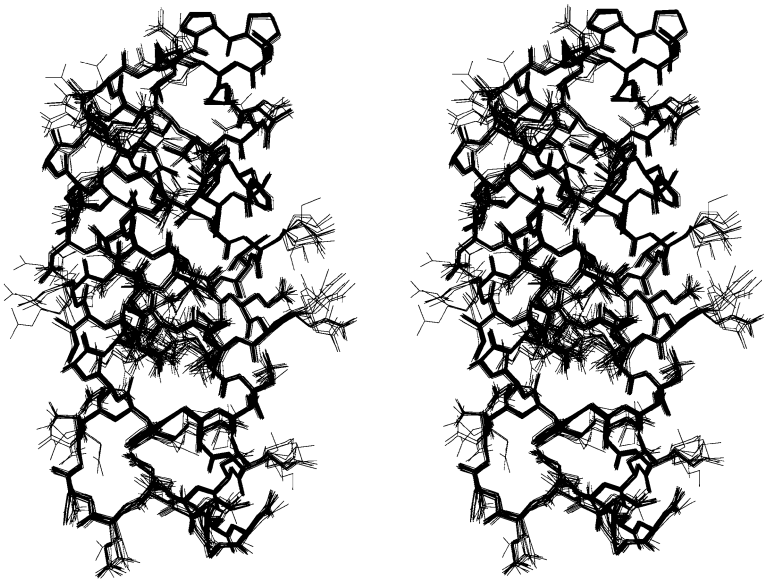

Figure 6. Ensemble of 20 D1 non-hydrogen structures of ordered region (22-89) with neither NOE nor dihedral angle violations > 0.5 Å or 5° respectively. The residues in the loop, including G66, L67, D68, E69, D70 and G71, are flexible based on our relaxation studies, and their RDCs were not used in the refinement.

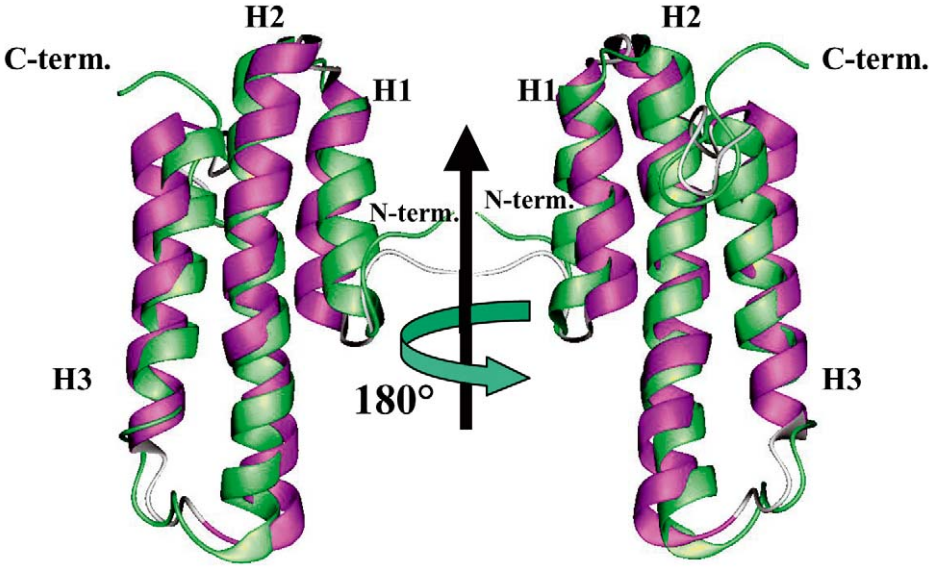

Figure 7. Comparison of ribbon diagrams of the minimized average structures of D1 determined using constraints, including two sets of RDCs (green), and that using homo-nuclear NMR (1NRE) (pink). The left and right views are rotated around the Y-axis by ca. 180° relative to each other. Although the local secondary structures are almost identical between the two structures, the helical orientations relative to each other are clearly different. The inter-helices angles were calculated using the program Interhlx (courtesy of K. Yap, University of Toronto): for the structure refined with RDCs, ⌞H1-H2 (angle formed by helix 1 and 2) = 173°, ⌞ H1-H3 = 7°, ⌞ H2-H3 = −166°; for 1NRE, ⌞H1-H2 = 165°, ⌞H1-H3 = 12°, ⌞H2-H3 = −164°. The sign of angles follows the definition by Drohat et al. (1996). Further, helix 2 of the NOE-based structure has a $\sim 15°$ curvature whereas it is relatively straight in the current structure. This curvature also contributes to the rmsd between the two structures (see the Figure 8).

well-defined region of D1 (23–88). The first helix starts at residue 23 and ends at residue 35, followed by a tight turn. The second helix is long and extends from residues 39 to 65, followed by the second turn (residues 66–71). The last helix consists of the residues 72–88. Overall, in terms of the local secondary structure, the current structure of D1 is very similar to the reported structure (accession no. 1NRE) (Nielsen et al., 1997). The main difference is the relative orientation among helices (see the next section), as we had expected.

PROCHECK (Laskowski et al., 1996) reveals that about 86% of D1 residues (18–98) have backbone torsion angles in the most popular region of the Ramachandran map. The percentage increases to ∼90% when only the ordered region (22–89) is used to calculate and when the Rama potential (Kuszewski et al., 1997) for driving backbone torsion angles to the most favored region in the map is turned off. The percentage reaches 96% when only the ordered region (22–89) is used to calculate and the Rama term is turned on. It is worthwhile to mention that the Q-factor decreases when Rama is turned on, indicating that the Rama term indeed improves the structure. The same result has been observed by Ramirez (Ramirez et al., 2000).

Helix orientation

RDCs measured in two alignment media provide important global restraints that complement translational and local restraints such as NOE and torsion angle restraints. The residual dipolar couplings measured in the two alignment media not only added more restraints to define the molecule and yield a better precision of the structure, but also provided a better accuracy of the determined structure (Tjandra and Bax, 1997). The changes in the quality of the structures are reflected not only in noticeable improvement in backbone rmsds relative to the average structure, but also in determining helix-to-helix orientation (Figures 6 and 7). Figure 8 illustrates C_α rmsd between the RDC refined structure and the homonuclear NOE-structure. The average rmsd between the two structures is ∼2 Å. It is noteworthy that the apparent ∼2 Å rmsd is significant when one considers that the average backbone rmsd among homologous proteins with ∼30–40% sequence identity is about 1–2 Å (Sali, 1999). This large rmsd mainly arises from the zigzag-variation in the rmsd vs. residue number, which simply reflects orientation differences in helices between the two structures.

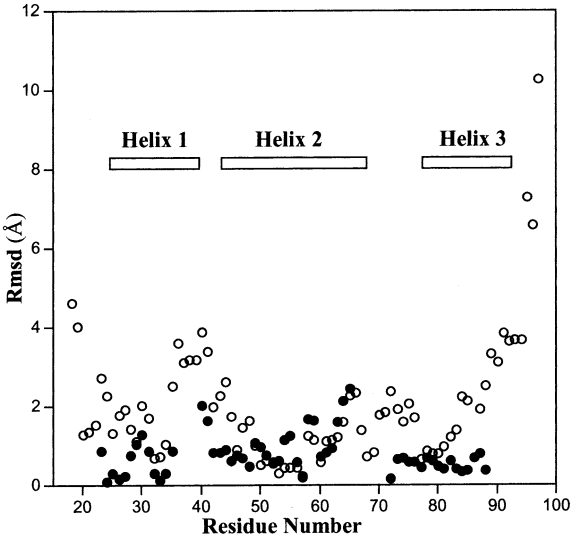

Figure 8. C_α rmsd (Å) between the current RDC refined structure (minimized average) and homo-nuclear NOE-based NMR structure vs. residue number. The average rmds is ∼2 Å if the two structures are aligned against each other (open circle), whereas the rmsd is under 1 Å between two structures if helices are aligned individually (filled circle). Also contributing to the overall rmsd difference between the two structures is the curvature (∼15°) observed in the NOE-based structure where it is relatively straight in the current structure.

The rmsd of individually aligned helices of the two structures is ∼0.7 Å. Further, helix 2 (residues 39-65) of NOE-based structure has an overall curvature of 15° whereas it is relatively straight in the current structure (Figure 7). As the result of the curvature, the rmsd between the two structures for this helix is relatively large comparing to the other two helices when helices are aligned individually (filled circle in Figure 8). These differences between the two structures could be partially due to different solution conditions or a slightly different protein construct used in studies. On the other hand, RDCs add global orientation constraints and complement NOE and torsion angle constraints in defining the angles between helices in this study and global orientation. Although in principle a structure with accurate helical orientations and curvature can be determined using extensive and accurately interpreted inter-helical NOEs, in practice it is almost impossible to obtain such a data set where spin diffusion, dynamics and extensive peak overlap certainly exist, and the application of RDCs becomes particularly useful in determining structures of proteins and especially helical bundle proteins. Moreover, RDCs are equally essential (Chou et al., 2002) in examining the detailed structural features such as

curvatures in peptides (Chou et al., 2002) where non-global types of constraints such as NOEs and dihedral angles are inadequate.

Conclusion

As the first step in our systematic studies towards the structure determination and understanding the interaction between RAP and members of the LDL receptor family, we have determined the solution structure of D1 using traditional NMR constraints together with RDCs measured in two independent alignment media. The C_α rmsd between the current structure and the homonuclear NOE based structure of D1 is $\sim$2 Å. This large rmsd mainly reflects the differences in helical orientation as well as curvature in helix 2 between the two structures. The determination of the current structure of D1 serves as the first step towards structure determination of the full-length RAP. The coordinates of the D1 NMR structure have been deposited in the Protein Data Bank under the code 1OP1.

Acknowledgements

We thank Drs Frank Delaglio and Dan Garrett for their assistance in NMRPipe and Pipp software; Drs G. Marius Clore, and Charles Schwieters for discussion about XPLOR-NIH; Mary Starich for maintaining the NMR spectrometers; R. Andrew Byrd for encouragement and helpful discussion; and Ms Carla Hemp for proof reading. This work was supported in part by grants HL50784, HL54710 and HL65939 to DKS from the National Institutes of Health.

Supporting materials

Supporting Information is available: Figure 1: Comparison of HSQC spectra of constructs D1, D2 and D12; Saupe matrix note: The irreducible representation of the Saupe order matrix.

References

Bax, A., Kontaxis, G. and Tjandra, N. (2001) In *Nuclear Magnetic Resonance of Biological Macromolecules*, Pt B, Vol. 339, pp. 127–174.

Chou, J.J., Gaemers, S., Howder, B., Louis, J.M. and Bax, A. (2001) *J. Biomol. NMR*, **21**, 377–382.

Chou, J.J., Kaufman, J.D., Stahl, S.J., Wingfield, P.T. and Bax, A. (2002) *J. Am. Chem. Soc.*, **124**, 2450–2451.

Clore, G.M., Gronenborn, A.M. and Bax, A. (1998a) *J. Magn. Reson.*, **133**, 216–221.

Clore, G.M., Gronenborn, A.M. and Tjandra, N. (1998b) *J. Magn. Reson.*, **131**, 159–162.

Cornilescu, G., Delaglio, F. and Bax, A. (1999) *J. Biomol. NMR*, **13**, 289–302.

Delaglio, F., Grzesiek, S., Vuister, G.W., Zhu, G., Pfeifer, J. and Bax, A. (1995) *J. Biomol. NMR*, **6**, 277–293.

Drohat, A.C., Amburgey, J.C., Abildgaard, F., Starich, M.R., Baldisseri, D. and Weber, D.J. (1996) *Biochemistry*, **35**, 11577–11588.

Garrett, D.S., Powers, R., Gronenborn, A.M. and Clore, G.M. (1991) *J. Magn. Reson.*, **95**, 214–220.

Garrett, D. S., Seok, Y.J., Liao, D.I., Peterkofsky, A., Gronenborn, A.M. and Clore, G.M. (1997) *Biochemistry*, **36**, 2517–2530.

Janin, J. and Chothia, C. (1990) *J. Biol. Chem.*, **265**, 16027–16030.

Kounnas, M.Z., Moir, R.D., Rebeck, G.W., Bush, A.I., Argraves, W.S., Tanzi, R.E., Hyman, B.T. and Strickland, D.K. (1995) *Mol. Biol. Cell*, **6**, 1901–1901.

Kuszewski, J., Gronenborn, A.M. and Clore, G.M. (1997) *J. Magn. Reson.*, **125**, 171–177.

Medved, L. V., Migliorini, M., Mikhailenko, I., Barrientos, L.G., Llinas, M. and Strickland, D.K. (1999) *J. Biol. Chem.*, **274**, 717–727.

Mueller, G.A., Choy, W.Y., Skrynnikov, N.R. and Kay, L.E. (2000) *J. Biomol. NMR*, **18**, 183–188.

Nielsen, P.R., Ellgaard, L., Etzerodt, M., Thogersen, H.C. and Poulsen, F.M. (1997) *Proc. Natl. Acad. Sci. USA*, **94**, 7521–7525.

Nilges, M., Clore, G.M. and Gronenborn, A.M. (1988) *FEBS Lett.*, **239**, 129–136.

Ramirez, B.E., Voloshin, O.N., Camerini-Otero, R.D. and Bax, A. (2000) *Protein Sci.*, **9**, 2161–2169.

Sali, A. (1999) *Nature*, **402**, 23–26.

Sass, J., Cordier, F., Hoffmann, A., Rogowski, M., Cousin, A., Omichinski, J.G., Löwen, H. and Grzesiek, S. (1999) *J. Am. Chem. Soc.*, **121**, 2047–2055.

Schwieters, C.D., Kuszewski, J., Tjandra, N. and Clore, G.M. (2003) *J. Magn. Reson.*, **160**, 66–74.

Stein, E.G., Rice, L.M. and Brunger, A.T. (1997) *J. Magn. Reson.*, **124**, 154–164.

Tjandra, N. and Bax, A. (1997) *Science*, **278**, 1697–1697.

Van Uden, E., Mallory, M., Veinbergs, I., Alford, M., Rockenstein, E. and Masliah, E. (2002) *J. Neurosci.*, **22**, 9298–9304.

Vuister, G.W. and Bax, A. (1994) *J. Biomol. NMR*, **4**, 193–200.

Willnow, T.E., Armstrong, S.A., Hammer, R.E. and Herz, J. (1995) *Proc. Natl. Acad. Sci. USA*, **92**, 4537–4541.

Wu, Y., Migliorini, M., Yu, P., Strickland, D.K. and Wang, Y-X. (2003) *J. Biomol. NMR*, **26**, 187–188.